IEEE Access
Multidisciplinary | Rapid Review | Open Access Journal

Received August 16, 2019, accepted August 31, 2019, date of publication September 3, 2019,
date of current version September 23, 2019.

Digital Object Identifier 10.1109/ACCESS.2019.2939271

A Compact Low-Profile Ring Antenna With Dual Circular Polarization and Unidirectional Radiation for Use in RFID Readers

JIADE YUAN[1], SHIJI WU[1], ZHIZHANG CHEN[1,2], (Fellow, IEEE), AND ZHIMENG XU[1]
[1]College of Physics and Information Engineering, Fuzhou University, Fujian 350116, China
[2]Department of Electrical and Computer Engineering, Dalhousie University, Halifax, NS B3H 4R2, Canada

Corresponding authors: Jiade Yuan (yuanjiade@fzu.edu.cn) and Zhizhang Chen (z.chen@dal.ca)

This work was supported in part by the Natural Science Foundation of Fujian Province of China under Grant 2019J01638, and in part by the Science and Technology Project Plan of Fuzhou of China under Grant 2018-G-89.

ABSTRACT A compact low-profile square ring antenna with unidirectional radiation and dual circular polarization (CP) is proposed for uses in radio frequency identification (RFID) readers. A small size conducting plane are slotted and placed underneath the ring antenna as a reflector to achieve low profile and unidirectional radiation. A branch line coupler is meandered inside the ring radiator to save space and generate dual circular polarization. Four inverted L-shaped strips are introduced to overcome the negative effects of tight coupling between the radiator and reflector. The measured −10 dB impedance bandwidth of $|S_{11}|$, 3 dB axial ratio (AR) bandwidth and maximum gain are of 850-1060 MHz, 876-1084 MHz and 5.62dBi, respectively. The lowest measured gain values in RFID band of 900-930 MHz is 4.54dBi and the overall size is 0.31 $\lambda_0 \times 0.31\ \lambda_0 \times 0.034\ \lambda_0$ (λ_0 is denoted the wavelength at center frequency). The proposed antenna has not only the lowest profile but also the best overall performances. It is an excellent antenna that can be fitted where there is a limited space in RFID system.

INDEX TERMS Ring antenna, low profile, slotted reflector, circular polarization (CP), left-hand polarization (LP), right-hand polarization (RP), radio frequency identification (RFID).

I. INTRODUCTION

Radio frequency identification (RFID) systems are widely used in object tracking, product manufacture, sales, logistics, etc [1]–[3]. A compact RFID reader has the high demands for being easy to carry and use. Its antenna is expected to have unidirectional radiation, circular polarization, high gain and be of low-profile; they ensure not only reliable communications between RFID tags and readers but also small form factors, light weights and compactness.

Among all the antennas suitable for RFID systems, planar antennas are the good candidates. Two major types of them are microstrip patch and ring antennas. The microstrip ring antenna is the better candidate since its side length is about one quarter-wavelength and one half of the conventional patch antenna [4]–[6] when they both operate at its fundamental mode. The circular polarization can also be easily obtained with the ring antenna [7]–[9]. Moreover, compared with the common planar inverted F antenna (PIFA), the ring antenna has smaller volume (or form factor) and better symmetry of radiation pattern [10]. Therefore, we select the ring antenna as our choice for RFID readers.

The microstrip ring antenna has a narrow bandwidth, similar to the microstrip patch antenna [7]. To have a better bandwidth, a bidirectional ring antenna is introduced and a distance of about one quarter of the wavelength is kept between the ring (or radiator) and its reflector; however, the distance of one quarter of the wavelength is too large to meet the miniaturization requirement of compact RFID readers.

A few techniques have been reported that reduce the distance between a radiator and its reflector [11]–[16]. In [11], a low-profile unidirectional antenna using artificial magnetic conductor (AMC) reflector for 2G/3G/4G base stations is presented. The AMC surface is a periodic structure and each unit cell consists of a pair of crossed-stubs inside a slot. Compared with common conductor reflector, the profile height using AMC reflector can be reduced by half.

The associate editor coordinating the review of this manuscript and approving it for publication was Lin Peng.

In [12], [13], a circularly polarized unidirectional antenna is developed with the AMC as a reflector and its profile height is 0.16 λ_0 and 0.10 λ_0, respectively. In [14], a wideband multiple input multiple output (MIMO) patch antenna with an AMC ground plane is proposed. The relative bandwidth can reach 31% with the profile height of about 0.19 λ_0. However, AMC structures not only are more complex but also can cause loss of efficiency as they are built on dielectric substrates with periodic couplings.

In [15], a compact circularly-polarized ring antenna with unidirectional pattern is proposed. The profile height of $\lambda_0/16$ is achieved with a meandered ring which can act as an inductive Yagi-Uda reflector. The dual circular polarization is claimed to be achieved with two feeds. Unfortunately, the isolation between the two feeds, $|S_{21}|$, is not measured [15] to experimentally verify the antenna design. In [16], a wideband low-profile unidirectional antenna with profile height of 0.16 λ_0 is obtained using the resonance-based reflector; however, the profile heights are still relative larger, which cannot fully meet the requirements for future compact RFID devices.

In this paper, a novel low-profile square ring antenna is developed with introduction of a slotted conducting plane as the reflector to generate unidirectional radiation. To produce dual circular polarization, four inverted L-shaped strips are added which also allow the optimization of the axial ratio (AR) and isolation between the two feeds. The proposed antenna has a smaller form factor than the existing antennas and is very suitable for limited space-restrain RFID devices.

II. ANTENNA CONFIGURATION

The proposed antenna is composed of a square ring radiator and a slotted planar reflector which are printed on the upper-layer and lower-layer dielectric substrates, respectively, as shown in Fig. 1(a). The dielectric substrates are IT-8350G with relative permittivity of 3.5, loss tangent of 0.0025 and thickness of 0.504mm, and they are separated by the distance of h. The square ring acts as a radiator fed by a branch line coupler, as shown in Fig. 1(b). Four branch lines of the coupler are meandered to save the space such that the coupler can be fully placed inside the ring radiator. Four inverted L-shaped strips connect to the ring. A square patch with four symmetric slant corner-cuts is located underneath the branch lines of the coupler and it acts as the ground.

The reflector is printed on the lower dielectric substrate; it consists of four U-shaped strips, a cross strip and four small square patches; all of them are printed within the ring-shaped strip, as shown in Fig. 1(c). Alternatively, the proposed reflector shown in Fig. 1 (c) can be viewed as a square conducting plane with slots cuts. The slots on the reflector make the equivalent coupling capacitance between it and the ring radiator relatively small so that antenna performances become less sensitive to profile height h in comparisons with the conventional planar antennas that has a solid conducting plane reflector.

Any change of any geometrical parameter can affect the antenna performance. By optimizing the parameters with

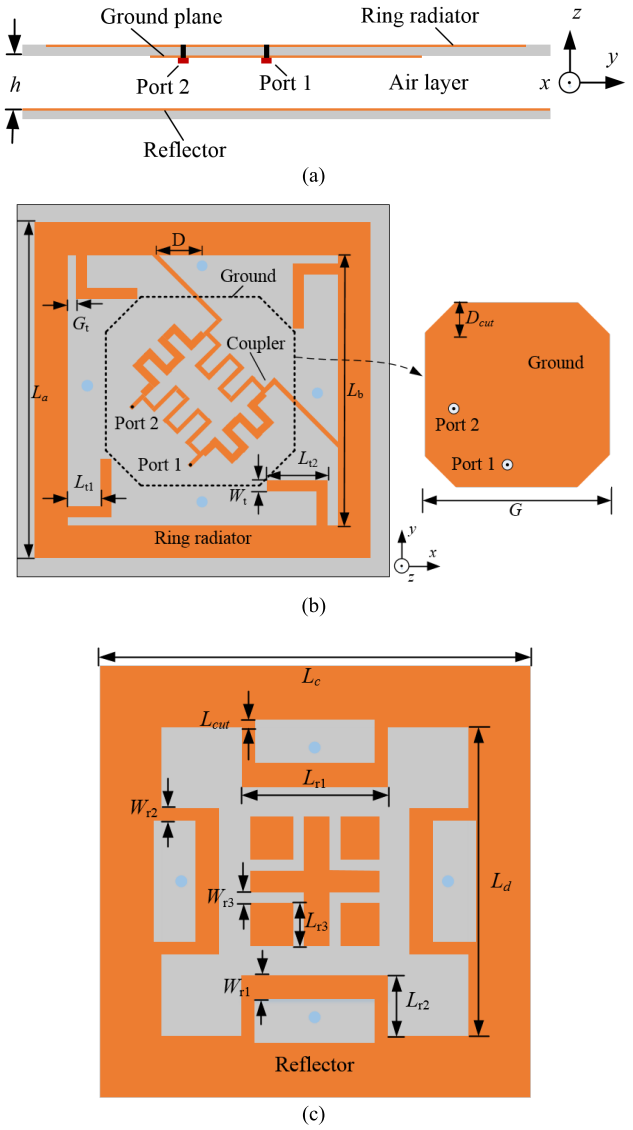

FIGURE 1. Geometry of the proposed antenna. (a) Cross sectional view, (b) top view (of the radiator), (c) bottom view (of the slotted ground reflector).

simulated software of ANSYS HFSS 18, geometrical parameters can be finalized and a compact low-profile antenna with dual circularly polarized unidirectional radiation properties can be obtained. The optimized dimensions of the proposed antenna are listed in Table 1. It should be noted here that port 1 and port 2 are diagonally symmetric in their positions. Therefore, we only need to examine the antenna performances with respect to port 1. In addition, the coupling or transmission between port 1 and port 2 represents the degree of the cross-polarization.

III. ANTENNA DESIGN AND ANALYSIS

In this section, design and analysis of the proposed antenna is presented. The resonant frequency of the square ring antenna can be estimated with the formula below [10]:

$$f_n = \frac{nc}{4L_a\sqrt{\varepsilon_{eff}}}, \quad n = 1, 2, 3 \ldots \tag{1}$$

TABLE 1. Optimized Geometric parameters (unit:mm).

Parameter	value	parameter	value	parameter	value
L_a	91	G	51	L_{r2}	8.3
L_b	73	D_{cut}	9.5	W_{r2}	3
L_{t1}	9	L_c	100	L_{r3}	10
L_{t2}	17	L_d	69.2	L_{cut}	0.9
W_t	3	L_{r1}	34	h	10
G_t	2.5	W_{r1}	5	D	11.5

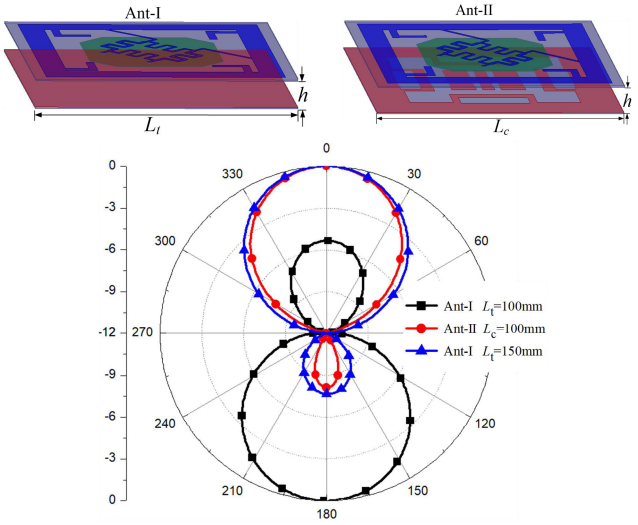

FIGURE 2. Radiation patterns with the proposed slotted reflector of L_c = 100mm and with the conventional solid planar reflector of L_t = 100mm, 150mm.

where c is the speed of electromagnetic wave in free space, L_a represents the side length of the square ring, ε_{eff} is the equivalent permittivity of the substrate, and n is the integer representing index of the antenna operating mode. In this paper, the proposed antenna is designed to operate at its fundamental mode ($n = 1$) with $L_a = \lambda_g/4$ (λ_g is the guided wavelength).

A. COMPACTNESS AND LOW-PROFILE

In principle, a unidirectional radiation antenna can be developed from a non-directional antenna by inserting a reflector with a distance of about $\lambda_g/4$ from the radiator of the antenna. Fig. 2 shows the two unidirectional antennas with reflectors and their performances. In the inset of Fig. 2, the antenna I (denoted as Ant-I) and antenna II (denoted as Ant-II) have the same radiator but with different types of reflector: Ant-I has a non-slotted solid conducting reflector with the side length of L_t while Ant-II has the proposed slotted conducting reflector with side length of L_c.

Fig. 2 shows the comparisons of the normalized directivity patterns of Ant-I and Ant-II with the same profile height of h = 10mm. It can be observed that Ant-II with the slotted reflector of L_c = 100mm can generates a much better directivity pattern than that of Ant-I with the same

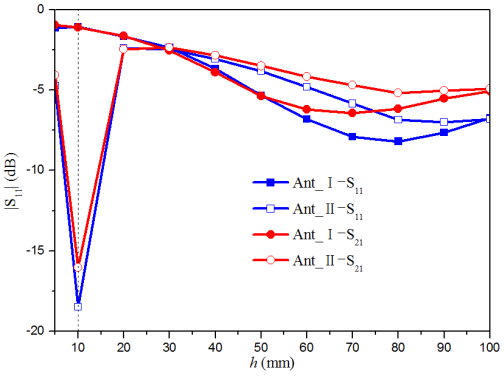

FIGURE 3. $|S_{11}|$ and $|S_{21}|$ for Ant-I and Ant-II versus profile height h.

size of L_t = 100mm. Moreover, to achieve the similar directivity, Ant-I needs to have a reflector of L_t = 150mm which is 50% larger in dimensions and 125% larger in area than Ant-II. In other words, Ant-II with the proposed slotted reflector is much more compact and smaller than Ant-I with the conventional solid reflector. The reason, as mentioned before, is that the slots in the reflector make the equivalent coupling capacitance between the radiator and the reflector relatively small so that antenna performances become relatively less sensitive to profile height h in comparisons with the conventional solid conducting plane reflector. The principle of unidirectional radiation of the proposed antenna is similar to that of the resonance based reflector in [17], [18], and the central structure of the slotted reflector is used to improve the unidirectional radiation or reduce the profile height.

The profile height of h is a crucial parameter on the antenna's form factor. It should as small as possible. However, with the decrease of h, the coupling electric field between the radiator and the reflector increases; and accordingly, the antenna performance will tend to deteriorate. Fig. 3 gives the $|S_{11}|$ and $|S_{21}|$ of Ant-I and Ant-II, respectively, when the h is first 5mm and then varied from 10mm to 100mm in a step of 10mm while L_t = 150mm and L_c = 100mm. As shown by the blue lines in Fig. 3, $|S_{11}|$ of Ant-I increase or deteriorate with decrease of h; or, $|S_{11}|$ of Ant-I decrease with increase of h but it levels off at its lowest value of about -8.2dB at about h = 80mm. In contrast, $|S_{11}|$ curve of Ant-II shows a sharply dip of $|S_{11}|$ to -18.5dB at h = 10mm where Ant-I has is only about -1.1dB of $|S_{11}|$. This proves that the slots in the reflector of Ant-II are effective, which can make the antenna low profile while deliver unidirectional radiation. This is because the slots can adjust the current flow paths and strengths and therefore current distributions in a proper manner such that good impedance matching is achieved without scarifying the radiation performances.

The isolation between port 1 and port 2, pertaining to the antenna cross-polarization, is measured as $|S_{21}|$; it is depicted with the red lines in Fig. 3 for both Ant-I and Ant-II. $|S_{21}|$ of Ant-I behaves similarly to its own $|S_{11}|$: it decreases and but levels off at about -6.4dB with increase of h. On the other hand, $|S_{21}|$ of Ant-II show a sharply dip -16.1 dB

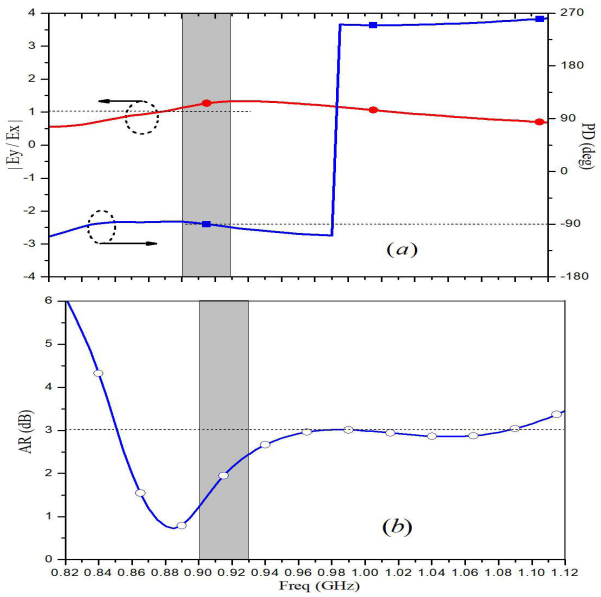

FIGURE 4. Simulation results of (a) amplitude ratios $|E_y|/|E_x|$ and PDs, (b) AR of far-field component $|E_y|$ and $|E_x|$ of the proposed antenna at the z-axis.

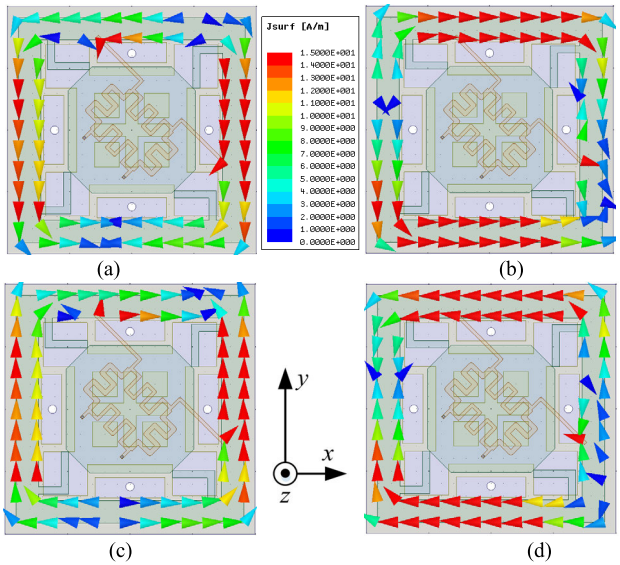

FIGURE 5. Simulated surface current distributions at the center frequency of 915MHz. (a) $\omega t = 0°$ (or $t = 0$), (b) $\omega t = 90°$ (or $t = T/4$), (c) $\omega t = 180°$(or $t = T/2$), (d) $\omega t = 270°$ (or $t = 3T/4$). T is the period of the signal.

at $h = 10$mm. Therefore, the best value of h for Ant-II is $h = 10$mm where Ant-II show much better performances than Ant-I.

B. DUAL CIRCULAR POLARIZATION

Circular polarization can be achieved only when the magnitudes of the two field components (i.e. $|E_y|$ and $|E_x|$) are equal and when their time-phase difference is an odd multiple of 90 degrees. That is

$$|E_\theta| = |E_\varphi|$$
$$\angle E_\theta - \angle E_\varphi = \begin{cases} +90°, & \text{for RHCP} \\ -90°, & \text{for LHCP} \end{cases} \quad (2)$$

A conventional 3dB branch-line coupler is utilized as a feed to the two orthogonal feeding ports with the identical magnitude and 90 degrees phase difference (PD), as shown in the inset of Fig. 1 (b). The size miniaturization of the coupler is achieved by meandering the branch line but keeps the total length of $\lambda_g/4$ unchanged. The probe feeds are set at port 1 and port 2, as shown in Fig. 1(b); the excitation at port 1 is to produce the right-hand circular polarization (RHCP) and the excitation at port 2 is to produce left-hand circular polarization (LHCP), respectively.

Fig. 4 (a) shows the ratio of the two orthogonal far-field electric fields, $|E_y|/|E_x|$, versus frequency for the proposed antenna at the boresight when port 1 is excited and port 2 is terminated with the matched load. It can be observed that the $|E_y|/|E_x|$ of the proposed antenna is closer to 1 in the RFID operating band of 902-928MHz. Meanwhile, Fig. 4 (a) shows the PD between the two orthogonal electric fields, and as seen, the PD of Radiator II is generally closer to 90 degrees. Therefore, better AR of Radiator II is achieved, as shown in the Fig. 4 (b).

The current density distributions at different time instants are also simulated and studied for further verification of the circular polarization performance. Fig. 5 shows the simulated currents at 915 MHz when port 1 is excited and port 2 is matched with 50Ω. As seen, the currents flow along the square ring as time t increases from $\omega t = 0°$ to $\omega t = 270°$ (ω is the angular frequency). At $t = 0$, the predominant currents on the right and left strips flow in the same $-y$ direction, as shown in Fig. 5 (a) and reinforce the far fields generated by each other. At the next time instant of $\omega t = 90°$, the currents on the top and bottom strips flow in the same +x direction, as shown in Fig. 5 (a), and reinforce the far fields generated by each other. As further seen from in Fig. 5 (c) and (d), the predominant currents at $t = 180°/\omega = T/2$ and $t = 270°/\omega = 3T/4$ are equal in magnitude and opposite in phase to the currents at $t = T/4$ and $t = T/2$, respectively.

In short, the vector sum of the predominant currents flow in the anticlockwise direction, from −y direction, to +x direction, to +y direction and then to −x direction. Consequently, a Right-hand circular polarization (RHCP) is generated in the half-space of $z > 0$ with port 1 being excited and port 2 matched with 50Ω. Similarly, a left-hand circular polarization (LHCP) radiation is produced in the half-space of $z > 0$ when port 2 is excited and port 1 is matched with 50Ω. Therefore, a dual circular polarization is achieved.

C. PARAMETRIC STUDIES

Parametric studies are performed by simulation of the antenna parameters of $|S_{21}|$ and AR. Unless indicated otherwise, only one geometrical parameter is varied each time and the rest parameters are kept unchanged in the following investigations.

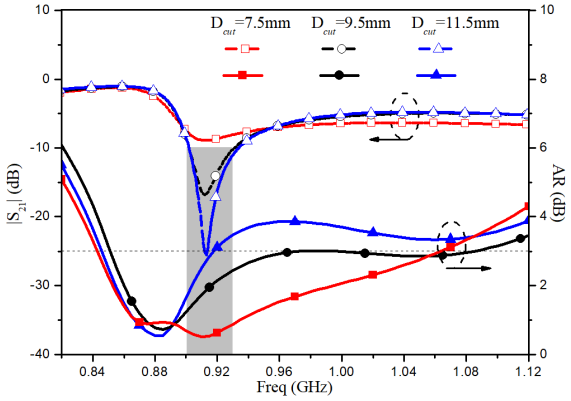

FIGURE 6. Variations of $|S_{21}|$ and AR with different dimensions of D_{cut}.

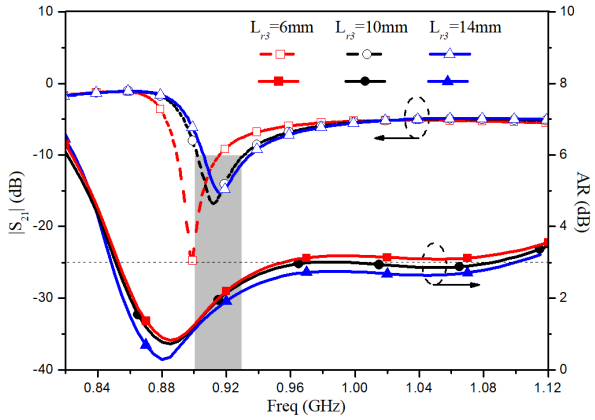

FIGURE 7. Variations of $|S_{21}|$ and AR with different dimensions of L_{r3}.

$|S_{21}|$ and AR at the boresight with varying depth of the slant corner-cuts of the coupler's ground, D_{cut}, are simulated and the results are show in Fig. 6. When D_{cut} increases from 7.5mm to 11.5mm with step length of 2mm, $|S_{21}|$ becomes better, while AR tends to become worse. The reason is that the coupling between the four inverted L-shaped strips and the slant corner-cuts ground is changed with the increases of D_{cut} and hence slightly changes the current distribution on the ring radiator. The optimal value is $D_{\text{cut}} = 9.5$mm.

The effects of the dimensions of the central structure of the slotted reflector, L_{r3}, on $|S_{21}|$ and AR are shown in Fig. 7. When L_{r3} increases from 6mm to 14mm with step length of 4mm, $|S_{21}|$ has quite variations and AR has slight variation; the lowest value of $|S_{21}|$ increases and shifts to the upper frequency. The reason can be due to the changes of mutual coupling between the ring radiator and the reflector. The optimal value is $L_{\text{r3}} = 10$mm.

IV. EXPERIMENTAL RESULTS AND DISCUSSIONS

With the optimized parameters as listed in Table 1, the proposed antenna is fabricated. The photo of the prototype is shown in Fig. 8 where the two layers are separated and supported with four plastic posts.

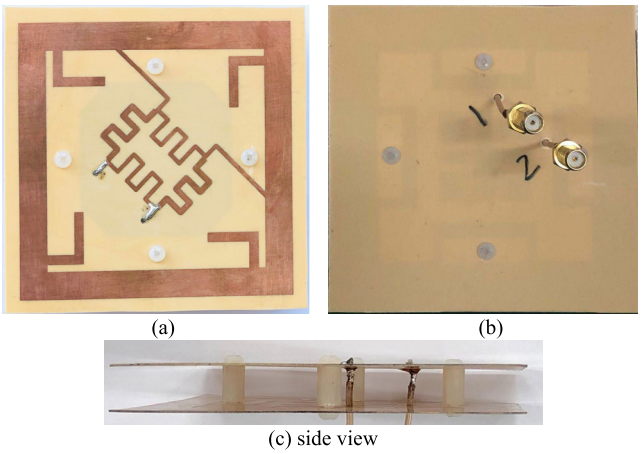

FIGURE 8. The fabricated prototype of the proposed antenna. (a) Top view, (b) bottom view, and (c) side view.

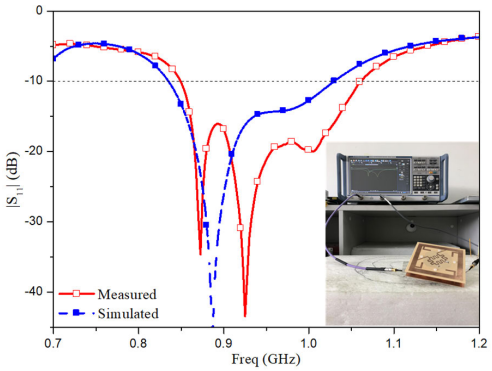

FIGURE 9. Simulated and measured $|S_{11}|$ of the proposed antenna.

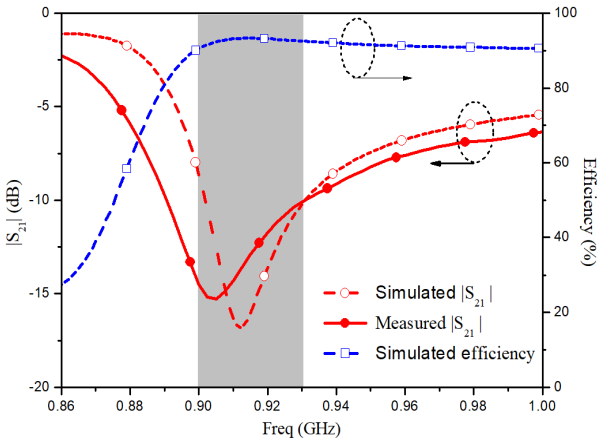

FIGURE 10. Simulated and measured $|S_{21}|$ and efficiency.

The prototype antenna was measured with Agilent E5071C vector network analyzer for S parameters and in our anechoic chamber for radiation pattern and AR. The tested and simulated results of the reflection coefficient of $|S_{11}|$ are shown in Fig. 9. The measured results show good corroborations with the simulated ones. The simulated -10 dB bandwidth of $|S_{11}|$ ranges from 836MHz to 1029 MHz and

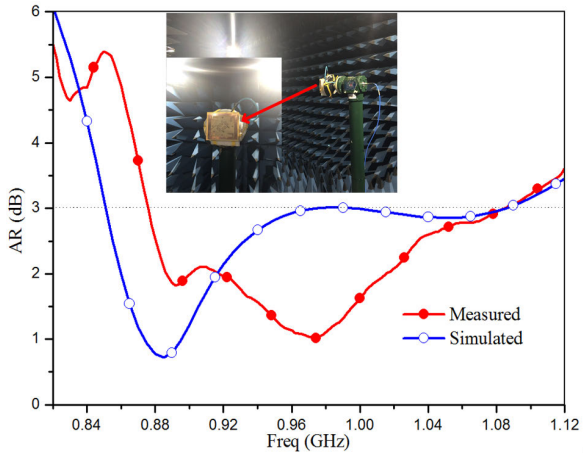

FIGURE 11. Simulated and measured AR and gain of the proposed antenna when port 1 is excited and port 2 is matched.

the measured bandwidth ranges from 850MHz to 1060 MHz which covers the full RFID operating bandwidth of 902-928MHz.

The measured and simulated transmission coefficient of $|S_{21}|$ and the simulated efficiency are shown in Fig. 10. The lowest measured $|S_{21}|$ is about -15.3dB and the simulated $|S_{21}|$ is about -16.8dB in the RFID frequency band. The simulated efficiencies are around 90% in the RFID operating band of 902-928 MHz. The measured and simulated AR at the boresight is shown in Fig. 11. The simulated 3dB AR bandwidth ranges from 855 MHz to 1085 MHz and the measured 3dB AR bandwidth ranges from 876 MHz to 1084 MHz, which fully covers the RFID frequency band of 902-928 MHz.

The total gain patterns at the frequency of 900MHz, 915MHz and 930MHz in the xz-plane and yz-plane are simulated and measured, respectively, and the results are shown in Fig. 12. It can be observed that the measured and simulated results have good corroborations. Fig. 13 gives the front gain (in z-axis direction), back gain (in the negative z-axis direction) and the front-to-back ratio (FBR) in the frequency band of 900-930MHz. It can be observed that the measured front gains and back gains are larger than 4.5dBi and less than -1.8dBi, respectively. The FBR in the RFID operating band are in the range of 6.61-7.55dBi. The simulated gain is 6.02dBi at $f = 900$MHz and increases to the maximum of 6.28dBi at $f = 908$MHz, and then drops to 5.13dBi at $f = 930$MHz. The measured gain is 5.62, 4.89 and 4.54 dBi at the frequency of 900, 915 and 930 MHz, respectively. They indicate that the proposed antenna has good directionality even it is of low profile. The differences between the measured and simulated results are due to the fabrication tolerance and the errors in measurement and simulation.

Sizes versus performances is one of the design indicators of an antenna [19], [20]. Table 2 shows the comparison of the antenna polarization mode (CP or linear polarization, LP), port numbers (PN), maximum measured gain, impedance bandwidth (IBW), reflector area, profile height

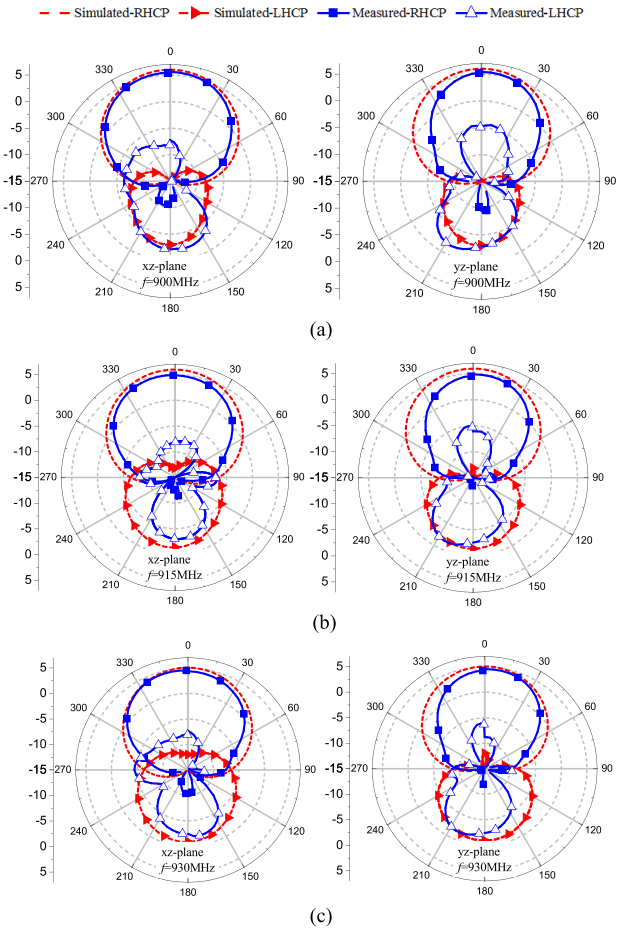

FIGURE 12. Measured and simulated radiation patterns at (a) 900 MHz, (b) 915MHz, (c) 930MHz. Port 1 is excited and port 2 is matched.

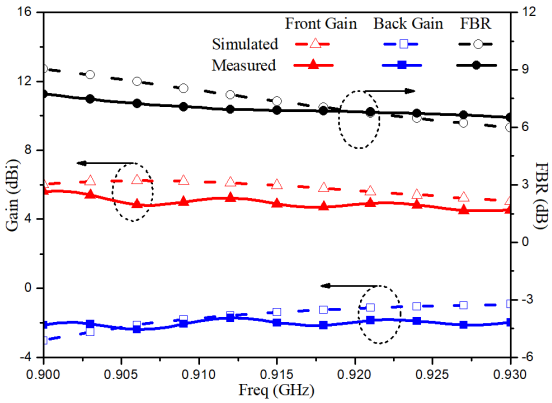

FIGURE 13. Simulated and measured front gain, back gain and FBR.

and the volume of the antennas in terms of the wavelengths between the proposed antenna and other recently-developed antennas. The volume comparison in terms of the wavelength is justifiable and representative since the antenna size is proportional to the wavelength or inversely proportional to the operational frequency.

TABLE 2. Comparison of the antenna size and refromances between the proposed and other existing antennas.

Ref.	Pol./#of Ports	Gain (dBi)	IBW (%)	Area (λ_0^2)	Height (λ_0)	Vol. (λ_0^3)
[11]	LP/2	7.30	45.5	1.10×1.39	0.143	0.2186
[12]	CP/1	5.50	15.9	0.54×0.54	0.080	0.0233
[13]	CP/1	6.60	46.9	0.94×0.94	0.050	0.0442
[14]	LP/2	7.10	31.0	0.89×0.89	0.20	0.1584
[15]	Dual CP/2	4.75	8.7	0.25×0.25	0.063	0.0039
[16]	LP/1	6.60	53.6	π×0.52^2	0.248	0.2106
This work	Dual CP/2	5.62	23.0	0.31×0.31	0.034	0.0033

The proposed antenna has the smallest profile height of 0.034 λ_0 and the volume of 0.0033λ_0^3 with a better measured gain of 5.62 dBi. Therefore, it is the antenna of the similar types that has the lowest profile and volume with good overall performances.

V. CONCLUSION

A compact low-profile dual circularly polarized ring antenna with unidirectional radiation has been developed for RFID applications. Several components, such as a slotted reflector, four inverted L-shaped strips and a meandered 3 dB coupler, are integrated to develop an antenna with a low profile of 0.034 λ_0 and a gain of 5.62 dBi in the RFID band. In particular, the introduction of the slotted reflector and the joint optimization of the radiator and reflector allow the development of a compact unidirectional antenna. The proposed antenna has the smallest profile height among the existing antennas of the similar types while maintain unidirectional radiation and adequate bandwidth. It promises to be a good antenna that can be used in compact RFID devices.

REFERENCES

[1] J.-H. Bang, C. Bat-Ochir, H.-S. Koh, E.-J. Cha, and B.-C. Ahn, "A small and lightweight antenna for handheld RFID reader applications," *IEEE Antennas Wireless Propag. Lett.*, vol. 11, pp. 1076–1079, 2012.
[2] M. Hyeon, Y. Sung, and E. Kim, "Dual-band circular polarised square-ring patch antenna loaded lumped capacitors," *IET Microw., Antennas Propag.*, vol. 12, no. 15, pp. 2326–2331, Dec. 2018.
[3] J. Zhang and Z. Shen, "Dual-band shared-aperture UHF/UWB RFID reader antenna of circular polarization," *IEEE Trans. Antennas Propag.*, vol. 66, no. 8, pp. 3886–3893, Aug. 2018.
[4] Nasimuddin, Z. N. Chen, and X. Qing, "Asymmetric-circular shaped slotted microstrip antennas for circular polarization and RFID applications," *IEEE Trans. Antennas Propag.*, vol. 58, no. 12, pp. 3821–3828, Dec. 2010.
[5] J. Li, H. Liu, S. Zhang, M. Luo, Y. Zhang, and S. He, "A wideband single-fed, circularly-polarized patch antenna with enhanced axial ratio bandwidth for UHF RFID reader applications," *IEEE Access*, vol. 6, pp. 55883–55892, 2018.
[6] M. Nestoros, M. A. Christou, and A. C. Polycarpou, "Design of wideband, circularly polarized patch antennas for RFID applications in the FCC/ETSI UHF bands," *Prog. Electromagn. Res. C*, vol. 78, pp. 115–127, 2017.
[7] J. S. Row, "Design of square-ring microstrip antenna for circular polarisation," *Electron. Lett.*, vol. 40, no. 2, pp. 93–95, Jan. 2004.
[8] Y. F. Lin, H. M. Chen, F. H. Chu, and S. C. Pan, "Bidirectional radiated circularly polarised square-ring antenna for portable RFID reader," *Electron. Lett.*, vol. 44, no. 24, pp. 1383–1384, Nov. 2008.
[9] J. Yuan, J. Zheng, and Z. D. Chen, "A compact meandered ring antenna loaded with parasitic patches and a slotted ground for global navigation satellite systems," *IEEE Trans. Antennas Propag.*, vol. 66, no. 12, pp. 6835–6843, Dec. 2018.
[10] K. Chen, J. Yuan, and X. Luo, "Compact dual-band dual circularly polarised annular-ring patch antenna for BeiDou navigation satellite system application," *IET Microw., Antennas Propag.*, vol. 11, no. 8, pp. 1079–1085, Jun. 2017.
[11] M. Li, Q. L. Li, B. Wang, C. F. Zhou, and S. W. Cheung, "A low-profile dual-polarized dipole antenna using wideband AMC reflector," *IEEE Trans. Antennas Propag.*, vol. 66, no. 5, pp. 2610–2615, May 2018.
[12] J. Li, H. Huo, J. Chen, S. Zhu, H. Shi, and A. Zhang, "Miniaturised artificial magnetic conductor and its application in unidirectional circularly polarised slot antenna design," *IET Microw., Antennas Propag.*, vol. 12, no. 12, pp. 1885–1889, Oct. 2018.
[13] W. Lin, S.-L. Chen, R. W. Ziolkowski, and Y. J. Guo, "Reconfigurable, wideband, low-profile, circularly polarized antenna and array enabled by an artificial magnetic conductor ground," *IEEE Trans. Antennas Propag.*, vol. 66, no. 3, pp. 1564–1569, Jan. 2018.
[14] J. Zhu, S. Li, S. Liao, and Q. Xue, "Wideband low-profile highly isolated MIMO antenna with artificial magnetic conductor," *IEEE Antennas Wireless Propag. Lett.*, vol. 17, no. 3, pp. 458–462, Mar. 2018.
[15] Y. Li, S. Sun, and F. Yang, "A miniaturized Yagi-Uda-oriented double-ring antenna with circular polarization and directional pattern," *IEEE Antennas Wireless Propag. Lett.*, vol. 12, pp. 945–948, 2013.
[16] L. Peng, J.-Y. Xie, X.-F. Li, and X. Jiang, "Front to back ratio bandwidth enhancement of resonance based reflector antenna by using a ring-shape director and its time-domain analysis," *IEEE Access*, vol. 5, pp. 15318–15325, 2017.
[17] L. Peng, J.-Y. Xie, K. Sun, X. Jiang, and S.-M. Li, "Resonance-based reflector and its application in unidirectional antenna with low-profile and broadband characteristics for wireless applications," *Sensors*, vol. 16, no. 12, p. 2092, Dec. 2019.
[18] B.-J. Wen, L. Peng, X.-F. Li, K.-S. Mo, X. Jiang, and S.-M. Li, "A low-profile and wideband unidirectional antenna using bandwidth enhanced resonance-based reflector for fifth generation (5G) systems applications," *IEEE Access*, vol. 7, pp. 27352–27361, 2019.
[19] A. D. Yaghjian and S. R. Best, "Impedance, bandwidth, and Q of antennas," *IEEE Trans. Antennas Propag.*, vol. 53, no. 4, pp. 1298–1324, Apr. 2005.
[20] C. Pfeiffer, "Fundamental efficiency limits for small metallic antennas," *IEEE Trans. Antennas Propag.*, vol. 65, no. 4, pp. 1642–1650, Apr. 2017.

JIADE YUAN received the M.Sc. degree from the University of Electronic Science and Technology of China, in 2007, and the Ph.D. degree from the Nanjing University of Aeronautics and Astronautics, China, in 2010. Since 2013, he has been an Associate Professor with Fuzhou University, China. His current research interests include antennas and microwave devices.

SHIJI WU was born in Ningde, Fujian, China, in 1993. He received the B.S. degree in communication engineering from the North China Institute of Science and Technology, Langfang, China, in 2017. He is currently pursuing the M.S. degree with Fuzhou University, China. His current research interest includes antenna design and its applications for RFID systems.

ZHIZHANG (DAVID) CHEN (S'92–M'92–SM'96–F'10) received the master's degree in radio engineering from Southeast University, China, the Ph.D. degree in electrical engineering from the University of Ottawa, Canada. He was a NSERC Postdoctoral Fellow with McGill University, Montreal, Canada, in 1993. He was one of the originators of the unconditionally stable methods that have been highly cited and used. He and his team also developed a number of nonlinear ultra-wideband receivers and planar wireless power transfer transmitting and receiving structures. He has been an Adjunct or a Visiting Professor with the University of Nottingham, U.K., the École Nationale Supérieure des Télécommunications de Bretagne, France, Shanghai Jiao Tong University, the Beijing University of Aeronautics and Astronautics, Fuzhou University, the Hong Kong University of Science and Technology, and the University of Electronic Science and Technology of China. He is currently a Professor with Dalhousie University, Halifax, Canada, where he has served as the Head of the Department of Electrical and Computer Engineering. He has authored or coauthored more than 350 journal and conference articles in computational electromagnetics, RF/microwave electronics, antennas, and wireless technologies. His current research interests include time-domain electromagnetic modeling techniques, ultra-wideband wireless communication systems, and wireless power transfer. He is a Fellow of the Canadian Academy of Engineering and the Engineering Institute of Canada. He was a recipient of the 2005 Nova Scotia Engineering Award, the 2006 Dalhousie Graduate Teaching Award, the 2007 and 2015 Dalhousie Faculty of Engineering Research Award, the 2013 IEEE R. A. Fessenden Medal, and the Dalhousie University Professorship.

He was involved in organizing in many international workshops and conferences as the Chair, the Co-Chair, a session organizer, and a committee member. He has been an Associate Editor of the recently founded the IEEE JOURNAL ON MULTISCALE AND MULTIPHYSICS COMPUTATIONAL TECHNIQUES, since 2016, and the Guest Editor of several professional journals and magazines. He has been invited to give many invited talks and plenary speeches at various international meetings, conferences, and forums.

ZHIMENG XU received the B.Sc. degree in radio physics from Lanzhou University, China, in 2002, the M.Sc. degree in information and communication engineering from Xidian University, in 2005, and the Ph.D. degree in information and communication engineering from Fuzhou University, Fuzhou, China, in 2013. He was with the Department of Electrical and Computer Engineering, Dalhousie University, Canada, as a Postdoctoral Fellow, from March 2016 to March 2017, and a Visiting Scholar with the Department of Technology, University of Northern Iowa, from August 2011 to January 2012. He is currently an Associate Professor with Fuzhou University. His research interests include ultra-wideband technologies, wireless sensing technologies, and wireless information and power transfer technologies.